NOAA Technical Report NESS 77

Wind Analysis by Conditional Relaxation

Washington, D.C.
January 1979

U.S. DEPARTMENT OF COMMERCE
National Oceanic and Atmospheric Administration
National Environmental Satellite Service

NOAA TECHNICAL REPORTS

National Environmental Satellite Service Series

...ental Satellite Service (NESS) is responsible for the establishment and operation ...tellite systems of NOAA.

...rt in NOAA Technical Report NESS series will not preclude later publication in an ...rm in scientific journals. NESS series of NOAA Technical Reports is a continua- ... the consecutive numbering sequence of, the former series, ESSA Technical Report ... Satellite Center (NESC), and of the earlier series, Weather Bureau Meteorological ... (MSL) Report. Reports 1 through 39 are listed in publication NESC 56 of this series.

Reports in the series are available from the National Technical Information Service (NTIS), U.S. Department of Commerce, Sills Bldg., 5285 Port Royal Road, Springfield, VA 22161, in paper copy or microfiche form. Order by accession number, when given, in parentheses. Beginning with 64, printed copies of the reports, if available, can be ordered through the Superintendent of Documents, U.S. Government Printing Office, Washington, DC 20402. Prices given on request from the Superintendent of Documents or NTIS.

ESSA Technical Reports

NESC 43 Atlas of World Maps of Long-Wave Radiation and Albedo--for Seasons and Months Based on Measurements From TIROS IV and TIROS VII. J. S. Winston and V. Ray Taylor, September 1967, 32 pp. (PB-176-569)

NESC 44 Processing and Display Experiments Using Digitized ATS-1 Spin Scan Camera Data. M. B. Whitney, R. C. Doolittle, and B. Goddard, April 1968, 60 pp. (PB-178-424)

NESC 45 The Nature of Intermediate-Scale Cloud Spirals. Linwood F. Whitney, Jr., and Leroy D. Herman, May 1968, 69 pp. plus appendixes A and B. (AD-673-681)

NESC 46 Monthly and Seasonal Mean Global Charts of Brightness From ESSA 3 and ESSA 5 Digitized Pictures, February 1967-February 1968. V. Ray Taylor and Jay S. Winston, November 1968, 9 pp. plus 17 charts. (PB-180-717)

NESC 47 A Polynomial Representation of Carbon Dioxide and Water Vapor Transmission. William L. Smith, February 1969 (reprinted April 1971), 20 pp. (PB-183-296)

NESC 48 Statistical Estimation of the Atmosphere's Geopotential Height Distribution From Satellite Radiation Measurements. William L. Smith, February 1969, 29 pp. (PB-183-297)

NESC 49 Synoptic/Dynamic Diagnosis of a Developing Low-Level Cyclone and Its Satellite-Viewed Cloud Patterns. Harold J. Brodrick and E. Paul McClain, May 1969, 26 pp. (PB-184-612)

NESC 50 Estimating Maximum Wind Speed of Tropical Storms From High Resolution Infrared Data. L. F. Hubert, A. Timchalk, and S. Fritz, May 1969, 33 pp. (PB-184-611)

NESC 51 Application of Meteorological Satellite Data in Analysis and Forecasting. Ralph K. Anderson, Jerome P. Ashman, Fred Bittner, Golden R. Farr, Edward W. Ferguson, Vincent J. Oliver, Arthur H. Smith, James F. W. Purdom, and Rance W. Skidmore, March 1974 (reprint and revision of NESC 51, September 1969, and inclusion of Supplement, November 1971, and Supplement 2, March 1973), pp. 1--6C-18 plus references.

NESC 52 Data Reduction Processes for Spinning Flat-Plate Satellite-Borne Radiometers. Torrence H. MacDonald, July 1970, 37 pp. (COM-71-00132)

NESC 53 Archiving and Climatological Applications of Meteorological Satellite Data. John A. Leese, Arthur L. Booth, and Frederick A. Godshall, July 1970, pp. 1-1--5-8 plus references and appendixes A through D. (COM-71-00076)

NESC 54 Estimating Cloud Amount and Height From Satellite Infrared Radiation Data. P. Krishna Rao, July 1970, 11 pp. (PB-194-685)

NESC 56 Time-Longitude Sections of Tropical Cloudiness (December 1966-November 1967). J. M. Wallace, July 1970, 37 pp. (COM-71-00131)

(Continued on inside back cover)

NOAA Technical Report NESS 77

Wind Analysis by Conditional Relaxation

Albert Thomasell, Jr.

Meteorological Satellite Laboratory
Washington, D.C.

January 1979

U.S. DEPARTMENT OF COMMERCE
Juanita M. Kreps, Secretary

National Oceanic and Atmospheric Administration
Richard A. Frank, Administrator

National Environmental Satellite Service
David S. Johnson, Director

CONTENTS

FIGURES

Figure No.		Page

WIND ANALYSIS BY CONDITIONAL RELAXATION

Albert Thomasell, Jr.
Meteorological Satellite Laboratory,
National Environmental Satellite Service, NOAA, Washington, D. C.

ABSTRACT. An objective wind analysis model for processing and evaluating satellite-derived winds is described in detail. Examples of applications of the model illustrate its adaptability to problems involving wind evaluation and the analysis and modification of wind fields.

1. INTRODUCTION

An objective wind analysis model developed at the Meteorological Satellite Laboratory provides a flexible research vehicle for processing and evaluating satellite-derived cloud motion wind vectors. The model is an adaptation of the Conditional Relaxation Analysis Method (CRAM) (Thomasell and Welsh 1963), a general purpose procedure for the two-dimensional objective analysis of any continuous scalar variable.

Model development began with a study to utilize wind observations for specifying upper-level reference heights for the recovery of height soundings from satellite measurements of radiance (Thomasell 1976a). Development continued with application of the model to the problem of determining the compatibility of satellite-measured low-level cloud motion wind vectors with rawins (Hubert and Whitney 1974). Further applications included a study to compare different objective techniques for calculating winds from cloud motion (Lemar and Bonner 1974); a study to define the wind field and the corresponding divergence and vorticity fields associated with easterly waves (Johnson 1976), using a dense network of low-level cloud motion vectors; and the development of an objective method for editing operational automated picture pair winds (Green et al. 1975, Thomasell 1976b).

This report describes the objective wind analysis model, illustrates some of its characteristics, and presents examples of typical applications.

2. THE ANALYSIS MODEL

A wind vector field is obtained by combining separate analyses of the u and v wind components calculated in spherical coordinates on the latitude-longitude grid described in appendix A. Analysis of a wind component field is accomplished in two steps. In one step, observations of the wind component are used to correct a first guess field at gridpoints nearest the observations. These corrected gridpoints are denoted internal boundary points. For many practical applications a first guess field is not readily available; for these cases a useful estimate may be obtained from existing observations by the method described in appendix B. In the next step, new values are interpolated for all points in the first guess field not identified as boundary points, making use of the information in the boundary values and in the first guess field. The resulting analysis may be smoothed, if needed, by the smoothing operator described in appendix C (for a comprehensive description of smoothing filters see Shuman (1957) and Thomasell et al. (1966).

2.1 Correction of First Guess With Observations

In the first analysis step the first guess field of each wind component is corrected by corresponding components of the observed winds. At the location of each observed wind component, which in general does not coincide with gridpoints, a value is obtained by bilinear interpolation from the first guess field. The difference between the observed and the interpolated wind components is added to the first guess value at the nearest gridpoint. If more than one wind observation affects a given gridpoint the average difference is added. Gridpoint values directly determined from winds by this correction procedure are called internal boundary values.

More than one group of winds may be used in the correction process, and each group may be assigned a unique relative weight. In this case a weighted average difference will comprise the correction and will determine the internal boundary value at each affected gridpoint.

2.2 Interpolation of Analysis Between Boundary Values

In the second analysis step the gridpoints in the analysis gridpoint array that were not directly affected by wind data (the nonboundary points, denoted by the grid indices I,J), are next assigned new values by forcing them to assume values that satisfy the Poisson equation

$$\nabla^2\phi(I,J) = F(I,J), \qquad (1)$$

where F, for forcing function, is defined as the Laplacian of the first guess field

$$F(I,J) = \nabla^2\phi_{FG}(I,J).$$

The parameter ϕ may be u or v depending upon which wind component is being analyzed. This use of a Poisson equation is simply a device to utilize the curvature in the first guess field, through the Laplacian to allow nonlinear interpolation between observations. The accuracy of the interpolated values will depend upon the accuracy of the curvature of the first guess field.

Equation (1) is solved by an iterative relaxation procedure, during which the internal boundary values and the peripheral boundary values are held fixed. For each nonboundary point in the grid array, compute a new value of ϕ according to

$$\phi(I,J)_N = \phi(I,J)_{N-1} + \alpha R(I,J)_{N-1} \qquad (2)$$

if the residual

$$R(I,J) = \nabla^2\phi(I,J) - F(I,J)$$

is greater than a sufficiently small value ε, the relaxation limit. The Laplacian is computed from the latest available values of ϕ for faster convergence. The subscripts in (2) refer to the iteration number. The parameter α is the relaxation coefficient and must be less than 0.5 for convergence. The iterations are continued until the residuals R are all equal to or less than ε or until a prescribed number of iterations is reached. Typically, $\varepsilon = 0.01$, $\alpha = 0.4$, and the number of iterations is approximately 40.

When the forcing function is set to zero, Poisson's equation reduces to Laplace's equation, the solution of which may be represented by a membrane stretched over the internal and peripheral boundary values. For this case, extrema can occur only at the boundary points. For a nonzero forcing function extrema can occur anywhere in the field.

2.3 Direction Dependent Pseudo Winds

Wind speed in general, tends to be more highly correlated along the wind direction than normal to it. This is more pronounced at higher levels where winds are stronger. A simple but effective method of incorporating this property of winds into the analysis model consists of calculating a pseudo wind upstream and downstream from each wind observation at a distance that is proportional to the observed wind speed. The pseudo winds are assigned a weight of 0.1 compared with 1.0 for observed winds. The pseudo winds comprise a distinct group of winds and may be used in the first guess correction process in the manner described in section 2.1.

3. AN EXAMPLE OF HIGH-LEVEL WIND ANALYSIS

In this section the importance of direction-dependent pseudo winds in high level wind analysis is demonstrated. Figure 1 (all the figures are presented in Mercator projection) shows the set of 300-mb rawins available over North America for February 23, 1975 at 1200 GMT. Figure 2 shows the same rawins (the larger barbs) and the pseudo winds calculated from them. For each rawin, two pseudo winds are generated, equal in speed and direction to the rawin, upstream and downstream from it. The displacement of the pseudo winds is proportional to the wind speed and in this case was set to one grid interval (2.5°) per 100 kt.

The wind analysis constructed from the basic set of rawins (fig. 1) is presented in figure 3. Figure 4 gives the wind analysis constructed from the rawins and pseudo winds from fig. 2. Because no first guess was available, it was necessary to generate one from the given data by the technique described in appendix B. The first guess was then smoothed with the filter discussed in appendix C. The analyses given in figures 3 and 4 were calculated using the procedures outlined in sections 2.1 and 2.2 and were smoothed with the same filter; however, in this final smoothing the boundary values defined by data were not allowed to be changed by the filter.

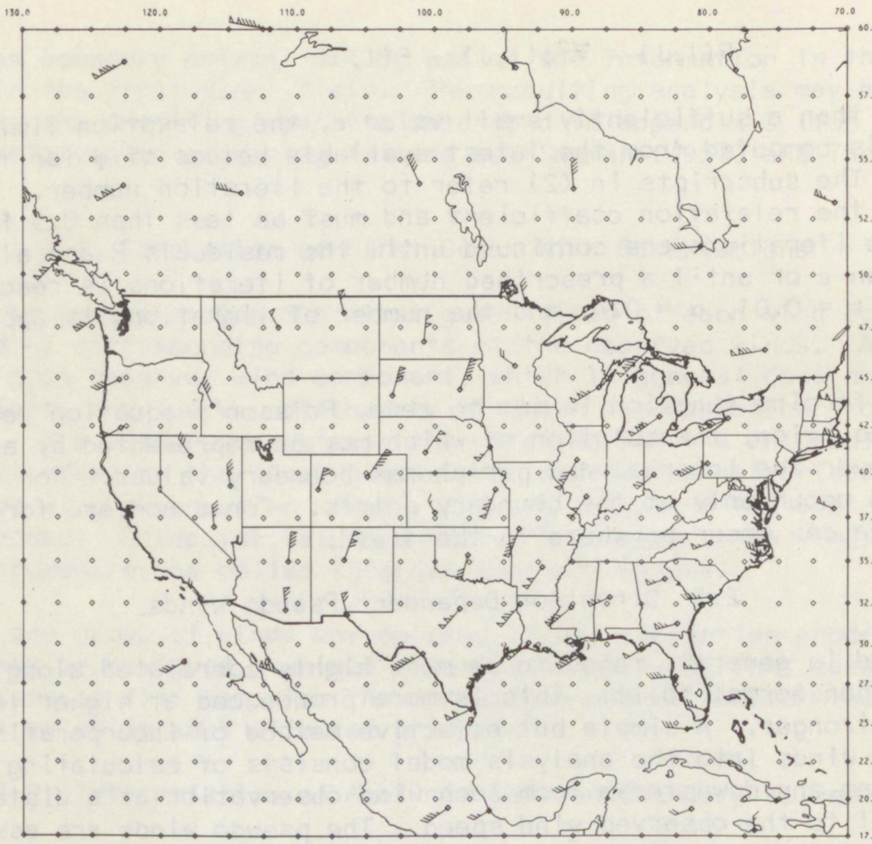

Figure 1. The 300-mb rawins for February 23, 1975 at 1200 GMT.

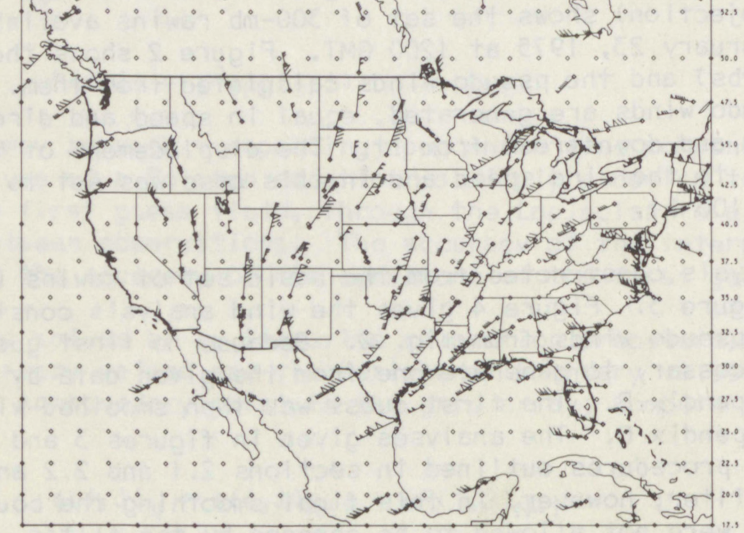

Figure 2.--The same rawins shown in figure 1 and the pseudo winds (smaller barbs) calculated from them.

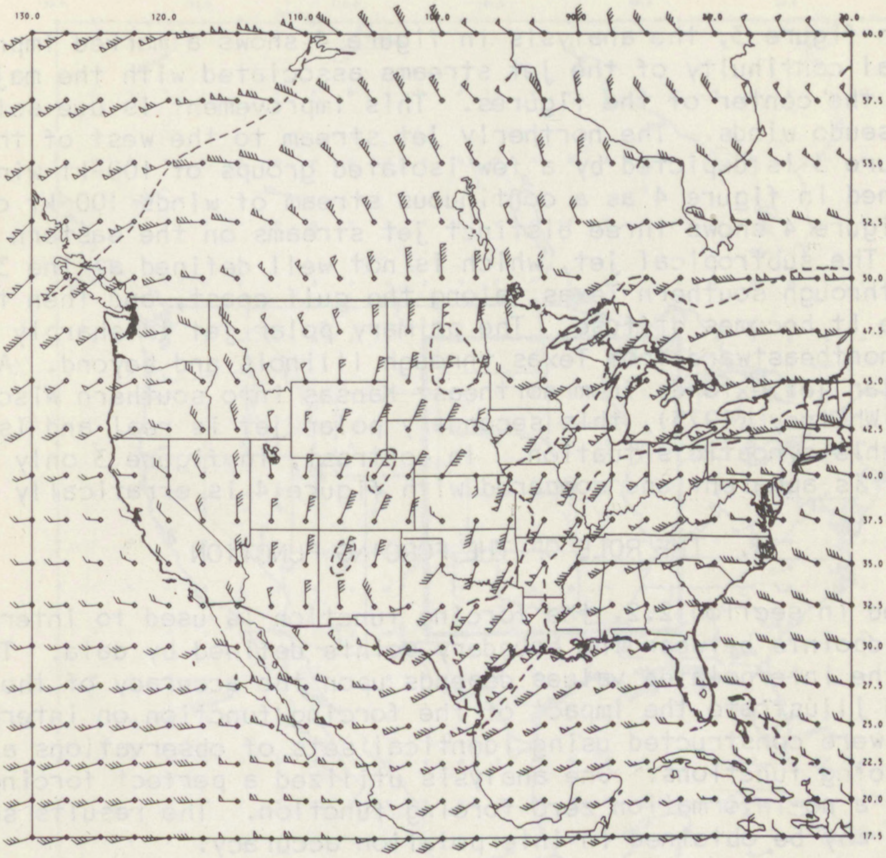

Figure 3. The wind analysis (100 kt isotachs) constructed from the rawins shown in figure 1.

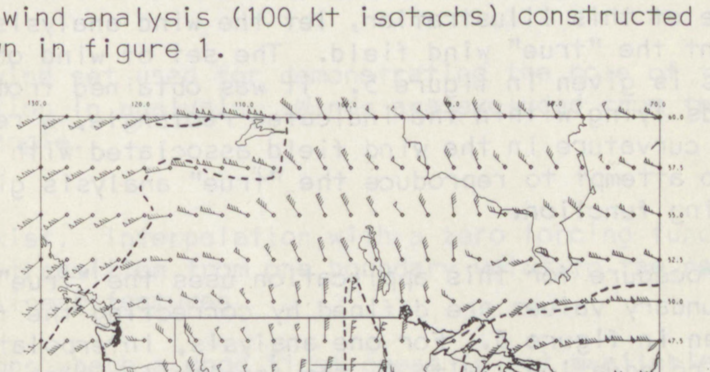

Figure 4. The wind analysis constructed (100 kt isotachs) from the rawins and pseudo winds shown in figure 2.

Compared with figure 3, the analysis in figure 4 shows a marked improvement in the spatial continuity of the jet streams associated with the major trough located near the center of the figures. This improvement is due solely to the use of pseudo winds. The northerly jet stream to the west of the trough, which in figure 3 is depicted by a few isolated groups of 100-kt winds, is clearly defined in figure 4 as a continuous stream of winds 100 kt or greater. Similarly, figure 4 shows three distinct jet streams on the eastern side of the trough. The subtropical jet, which is not well defined at the 300-mb level, runs through southern Texas, along the gulf coast, and then through Georgia where it becomes diffuse. The primary polar jet is sharply defined and extends northeastward from Texas through Illinois and beyond. A short secondary polar jet extends from northeast Kansas into southern Wisconsin. According to Whitney (1975), this secondary polar jet is real and is a common feature for this synoptic situation. In contrast, in figure 3 only the primary polar jet is apparent and compared with figure 4 is erratically defined.

4. THE ROLE OF THE FORCING FUNCTION

As described in section 2.2, the forcing function is used to interpolate values at gridpoints between the boundary points defined by data. The accuracy of the interpolated values depends upon the accuracy of the forcing function. To illustrate the impact of the forcing function on interpolation, two analyses were constructed using identical sets of observations and grossly differing forcing functions. One analysis utilized a perfect forcing function and the other a no-information zero forcing function. The results show the extremes that may be obtained in interpolation accuracy.

For the purpose of this illustration, let the wind analysis shown in figure 4 represent the "true" wind field. The set of wind observations used for both analyses is given in figure 5. It was obtained from figure 1 by removing the winds lying within the indicated rectangle, a region of strong shear and marked curvature in the wind field associated with the major trough. The problem is to attempt to reproduce the "true" analysis given the specified winds and a forcing function.

The analysis procedure for this application uses the "true" analysis for a first guess. Boundary values are defined by correcting the first guess with the wind set given in figure 5. For one analysis, interpolated values are computed by solving equation 1 with F, the forcing function, defined as the Laplacian of the "true" analysis. For the other analysis, equation 1 is solved with F set to zero. No final smoothing is applied to either analysis.

The wind analysis constructed with the "true" or perfect forcing function is shown in figure 6 and the vector difference between it and the "true" analysis is given in figure 7. Within the limits imposed by the relaxation solution of equation 1, figure 6 is seen to be a faithful reproduction of figure 4.

The analysis made with a zero forcing function is shown in figure 8 and its difference from the "true" analysis is given in figure 9. Substantial vector differences are seen throughout the entire analysis field in figure 9; in the data-void area centered on the trough, vector differences in excess of one

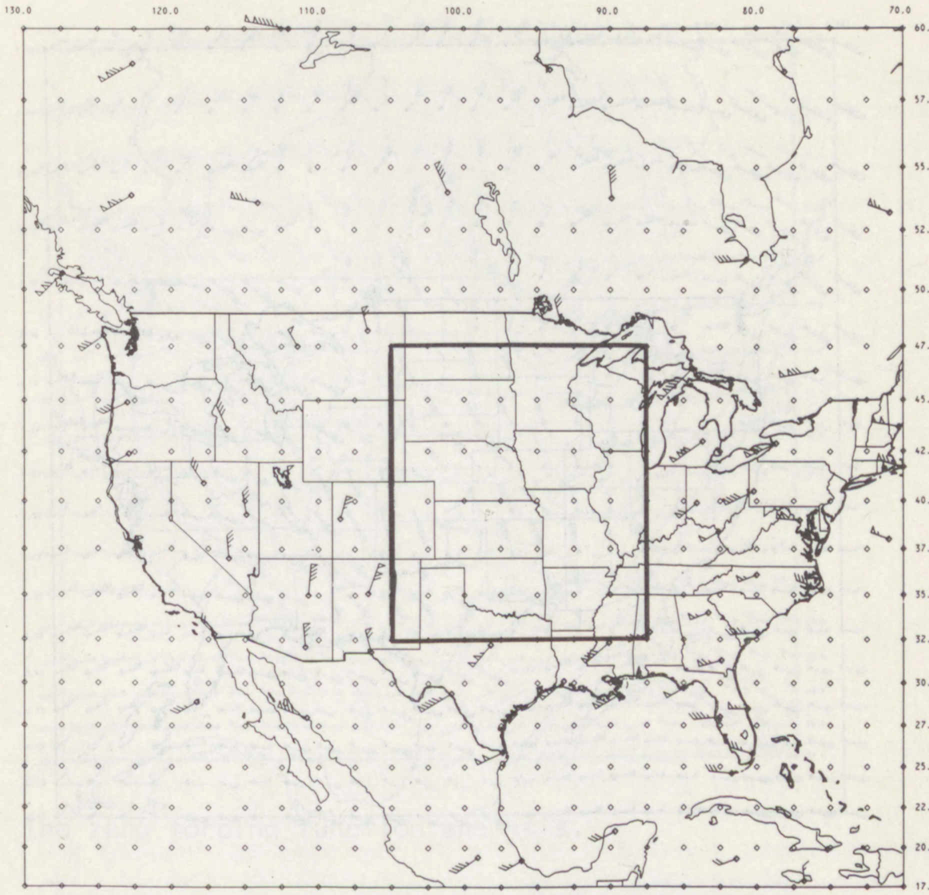

Figure 5. The wind set used for demonstrating the role of the forcing function in analysis. Winds are excluded from the inscribed rectangle.

hundred knots exist. Interpolation with a zero forcing function tends to effect a smooth transition from one boundary value to the next, and cannot define real nonlinear features.

For applications where a good first guess is not available, interpolation more closely resembles the zero forcing function case than the true forcing function case. In general, interpolation error is reduced as the distance between boundary values is reduced. The use of pseudo winds is one valid means of achieving lower interpolation errors.

5. OBJECTIVE EDITING

This section describes an application of the analysis model to the problem of objectively editing sets of low-level (900 mb) cloud motion wind vectors. It also serves to illustrate a typical low-level wind analysis constructed from cloud motion vectors and a reliable first guess, the related vorticity and divergence fields, the effect of operating on a scalar field with a smoothing filter, and the modification of a wind field to conform to prescribed vorticity and divergence fields.

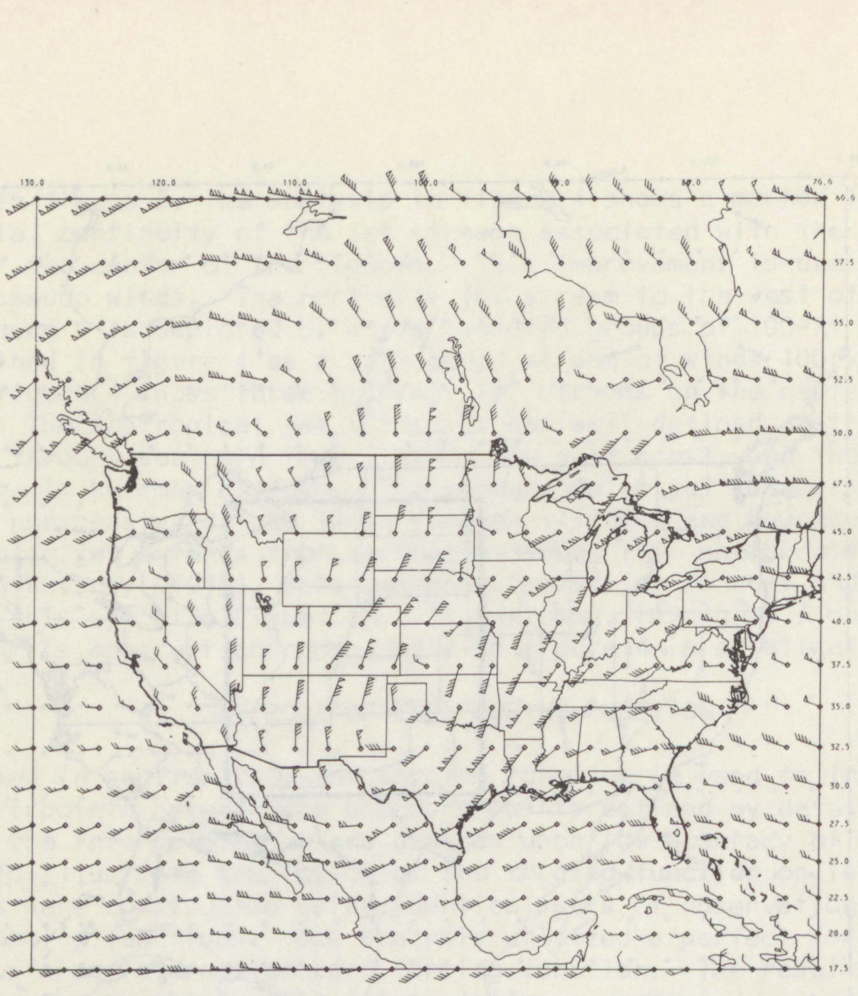

Figure 6. The perfect forcing function analysis.

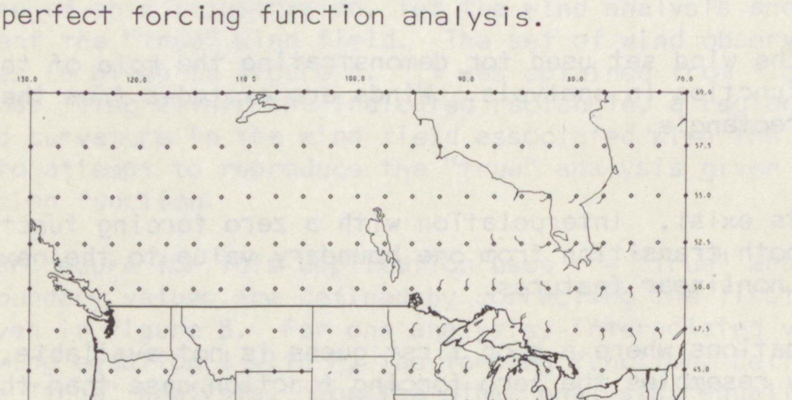

Figure 7. The vector error field of the perfect forcing function analysis compared with the "true" analysis shown in figure 4.

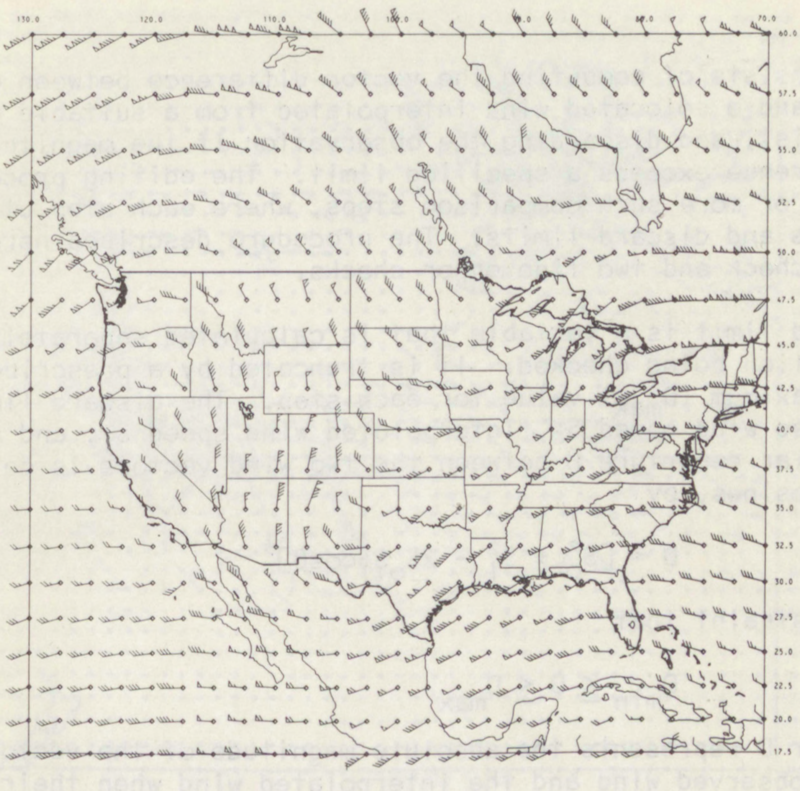

Figure 8. The zero forcing function analysis.

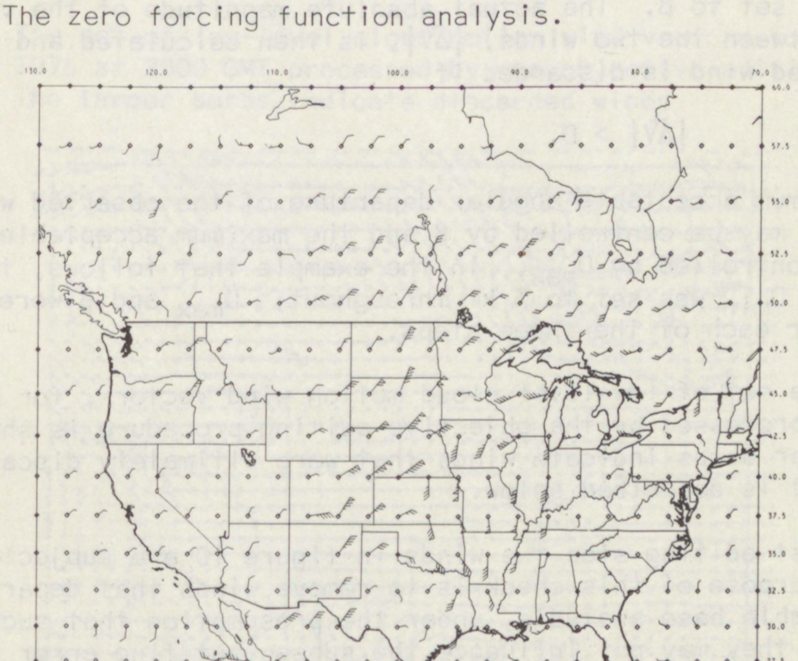

Figure 9. The vector error field of the zero forcing function analysis compared with the "true" analysis shown in figure 4.

Editing consists of computing the vector difference between each wind observation and a colocated wind interpolated from a suitable analyzed field (base analysis), and discarding the observation if the magnitude of the vector difference exceeds a specified limit. The editing procedure may comprise one or more such comparison steps, where each step utilizes its own base analysis and discard limits. The procedure described here involves one gross error check and two fine error checks.

The discard limit is a variable that is calculated separately for each wind observation being checked. It is truncated by a prescribed minimum (D_{min}) and maximum (D_{max}) value for each step. The discard limit D for a given observed wind speed S_O, interpolated wind speed S_I, and a prescribed maximum angular departure β between the two wind vectors is calculated using the law of cosines, by

$$D = [S_O^2 + S_I^2 - 2S_O S_I \cos\beta]^{\frac{1}{2}}$$

with the constraint that

$$D_{min} \leq D \leq D_{max}$$

The parameter D represents the absolute magnitude of the vector difference between the observed wind and the interpolated wind when their angular difference is set to β. The actual absolute magnitude of the vector difference between the two winds, $|\Delta\vec{V}|$, is then calculated and compared with D. An observed wind is discarded if

$$|\Delta\vec{V}| > D.$$

Thus the maximum acceptable angular departure of the observed wind from the base analysis may be controlled by β and the maximum acceptable difference in speed is controlled by D_{max}. In the example that follows, the minimum discard limit D_{min} was set to 3 kt throughout; D_{max} and β were specified separately for each of the three steps.

The complete set of low-level cloud motion wind vectors, for April 22, 1976 at 2000 GMT, processed by the objective editing procedure is shown in figure 10. The larger barbs indicate winds that were ultimately discarded by the procedure that is described below.

For the first editing step the winds in figure 10 are subjected to a gross check. The purpose of this check is to remove winds that depart markedly from a reasonable base analysis, under the presumption that such winds are erroneous, so they may not influence the subsequent fine error checks. To detect winds with gross departures, the base analysis must be independent of the winds being checked. This base analysis is constructed by using the NMC analysis shown in figure 11 (valid at 0000 GMT), as a first guess, and the latest error checked cloud motion winds, (in this case the 1500 GMT winds for April 22, 1976, shown in figure 12), and then applying the basic smoothing filter (appendix C). The resulting base analysis is shown in figure 13. For the gross check, the editing parameters are β = 90° and D_{max} = 28 kt. The winds discarded by the gross check are given in figure 14.

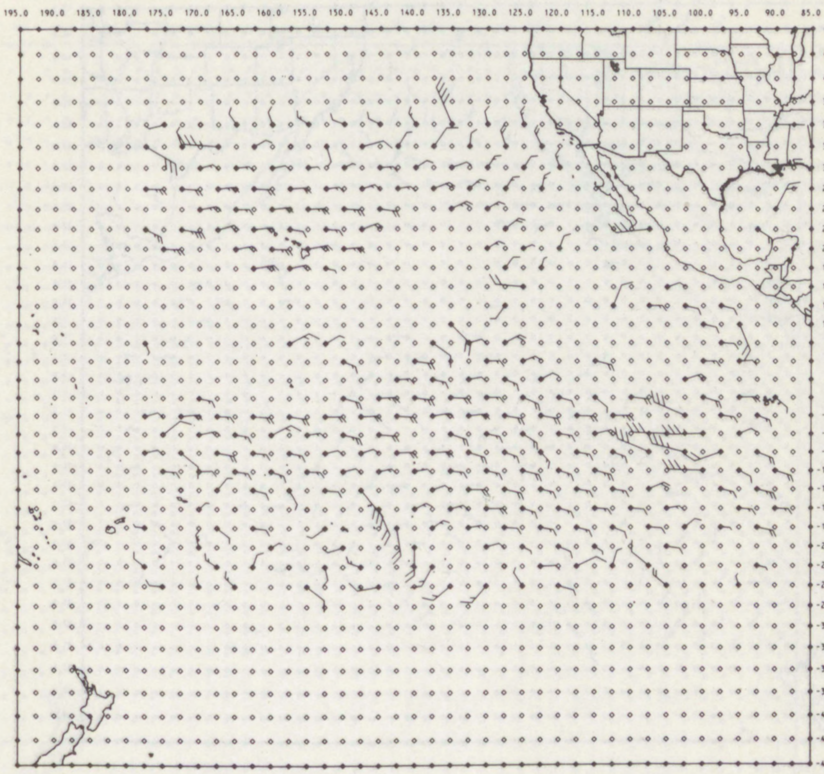

Figure 10. The set of low-level cloud motion wind vectors for April 22, 1976 at 2000 GMT processed by the objective editing procedure. The larger barbs indicate discarded winds.

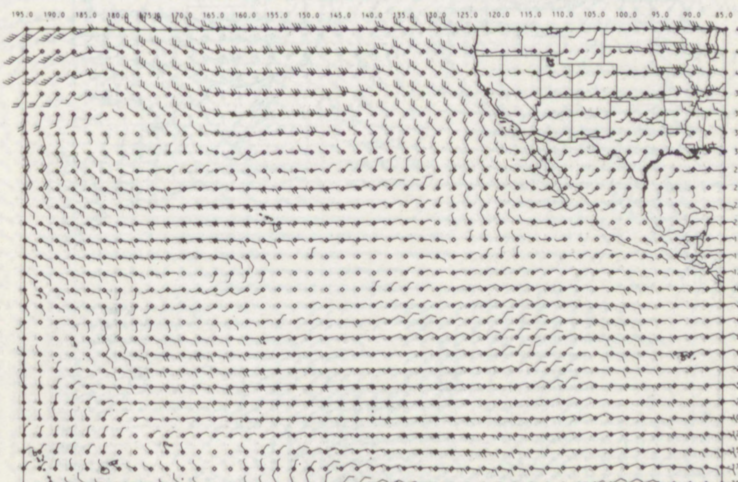

Figure 11. The NMC first guess wind field valid at April 22, 1976 at 0000 GMT.

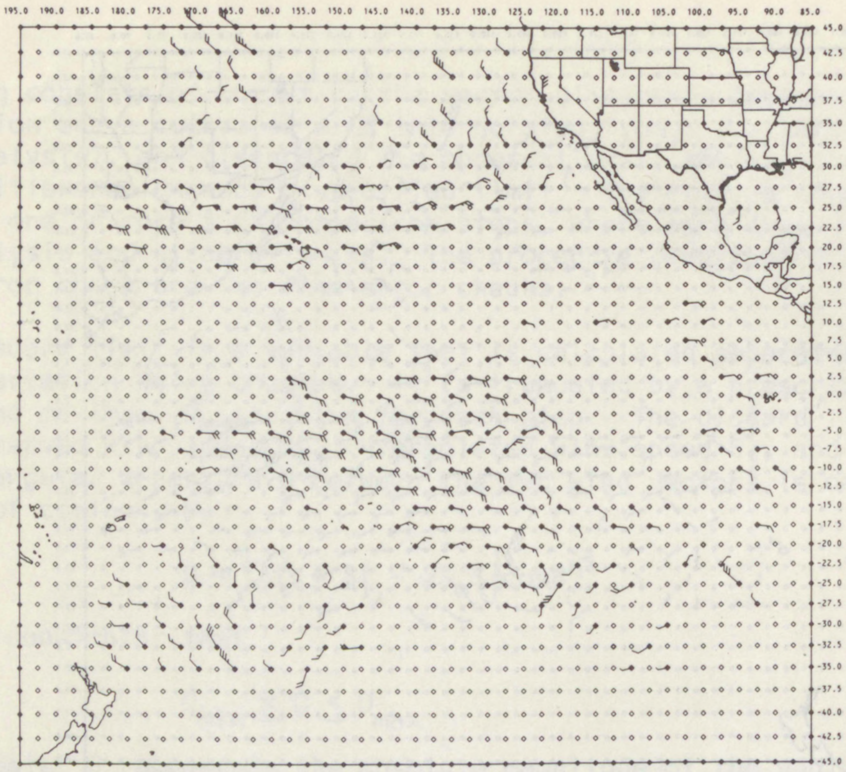

Figure 12. The set of error checked cloud motion winds for April 22, 1976 at 1500 GMT used for updating the NMC first guess.

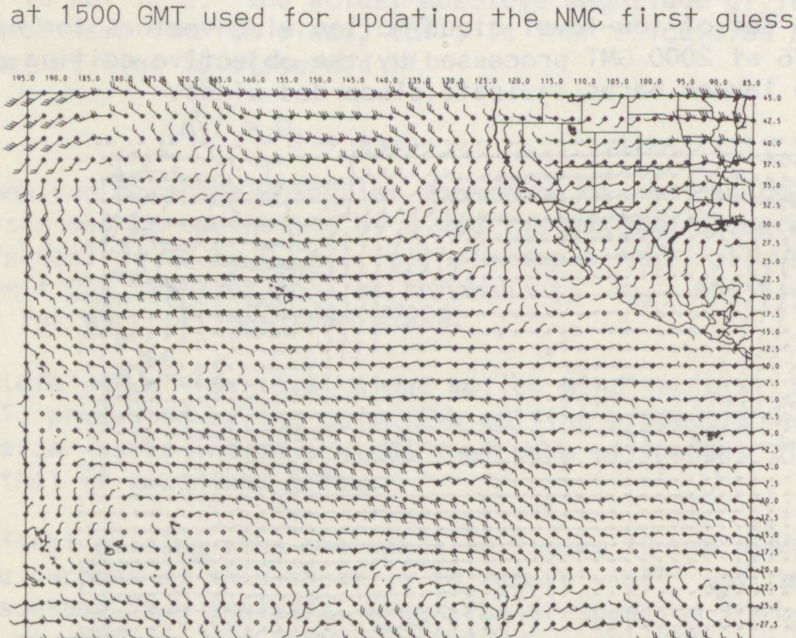

Figure 13. The base analysis used for the gross error check, constructed from the NMC first guess and the winds shown in figure 12.

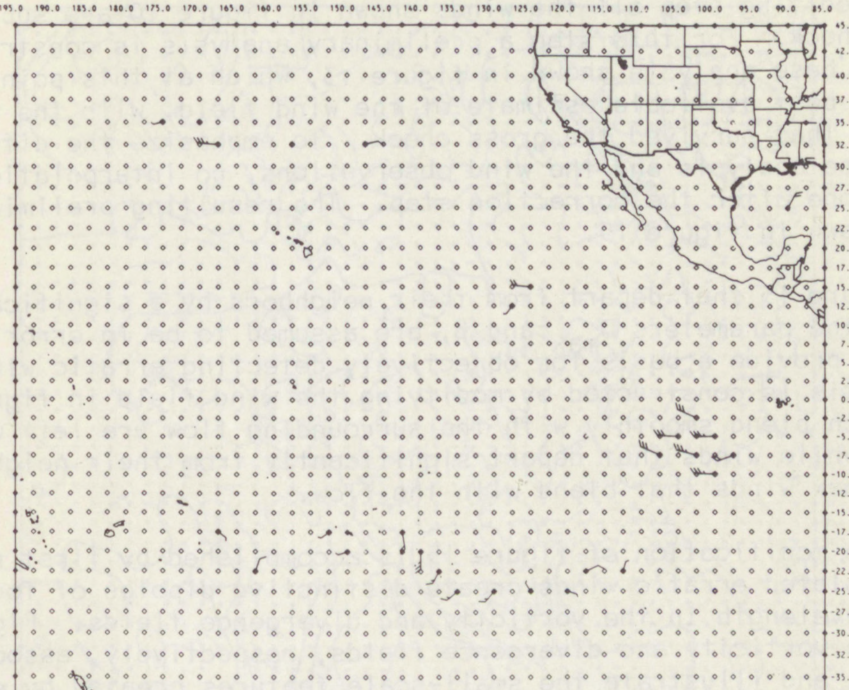

Figure 14. Winds from figure 10 that were rejected by the gross error check.

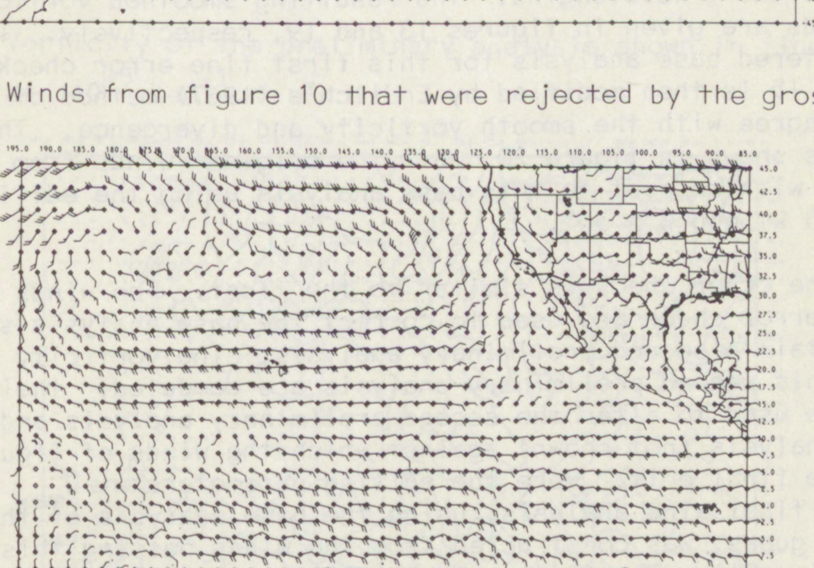

Figure 15. The preliminary analysis for the first fine error check, constructed by replacing winds in the base analysis of figure 13 with the winds from figure 10 that survived the gross error check.

In the next editing step all the winds shown in figure 10 are subjected to a fine error check. For this step a preliminary analysis is constructed by correcting the base analysis shown in figure 13, which at this point represents the best available estimate of the wind field, with the winds from figure 10 that survived the gross check. To emphasize the difference between the base analysis and the wind observations, no interpolation or smoothing is done after the correction step. The resulting preliminary analysis is shown in figure 15.

Winds in figure 15 that depart from their neighbors by a significant amount, as defined by the parameters D_{max} and β, are assumed to be in error and are discarded. To provide a basis for objectively detecting erratic winds, a new base analysis is constructed by modifying the wind field in figure 15 so that winds which blend smoothly with the surrounding flow are left with little change while winds that depart significantly from their neighbors are replaced with new winds that blend with the flow.

The selective modification of figure 15 is accomplished by first recognizing that isolated erratic winds create distinctive dipoles of four grid intervals in wavelength in the vorticity and divergence fields. Figures 16 and 17 show the vorticity and divergence fields, respectively, associated with figure 15, and illustrate the small-scale features created by erratic winds. The noisy vorticity and divergence fields are then smoothed with a filter to remove short wavelengths. The resulting smoothed vorticity and divergence fields are given in figures 18 and 19, respectively. To obtain the desired filtered base analysis for this first fine error check, the wind field in figure 15 is then modified by Endlich's (1967) method of altering wind fields to agree with the smooth vorticity and divergence. The resulting base analysis is shown in figure 20. All the original winds from figure 10 are then edited with respect to this base analysis using the editing parameters D_{max} = 15 kt and β = 30°.

The second fine error check is similar to the first. The winds surviving the first fine error check are used to correct the base analysis shown in figure 13 to obtain a second preliminary analysis. The vorticity and divergence of this second preliminary analysis are computed; their smoothed counterparts are used to alter the second preliminary analysis and generate a second base analysis (not shown) against which the winds of figure 10 are compared for the final edit. Here the editing parameters are D_{max} = 8 kt and β = 19°: A final wind analysis, using the base analysis of this last step as a first guess, was constructed from the winds passing this final editing step (fig. 21). The final set of edited winds is shown in figure 22.

6. SUMMARY

The objective wind analysis model described here produces reasonable and useful wind fields. The examples demonstrate that the model is adaptable to many problems involving wind analysis, wind evaluation, and manipulation of the kinematic properties of wind fields. The wind model is particularly useful as a research tool for processing satellite-derived cloud motion wind vectors.

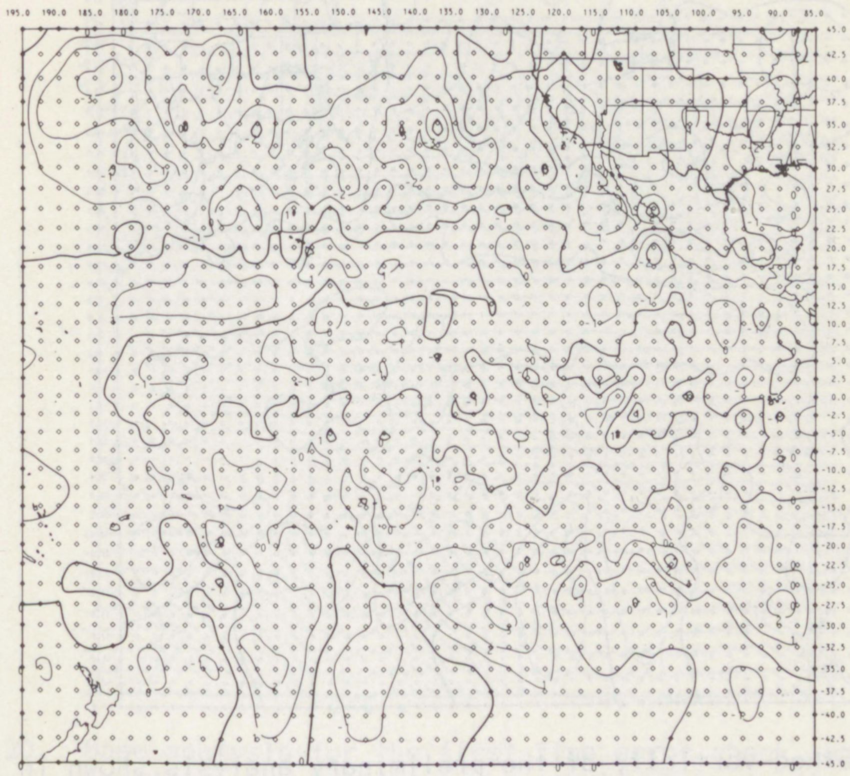

Figure 16. Vorticity of the preliminary analysis shown in figure 15. Units are 10^{-5} sec^{-1}.

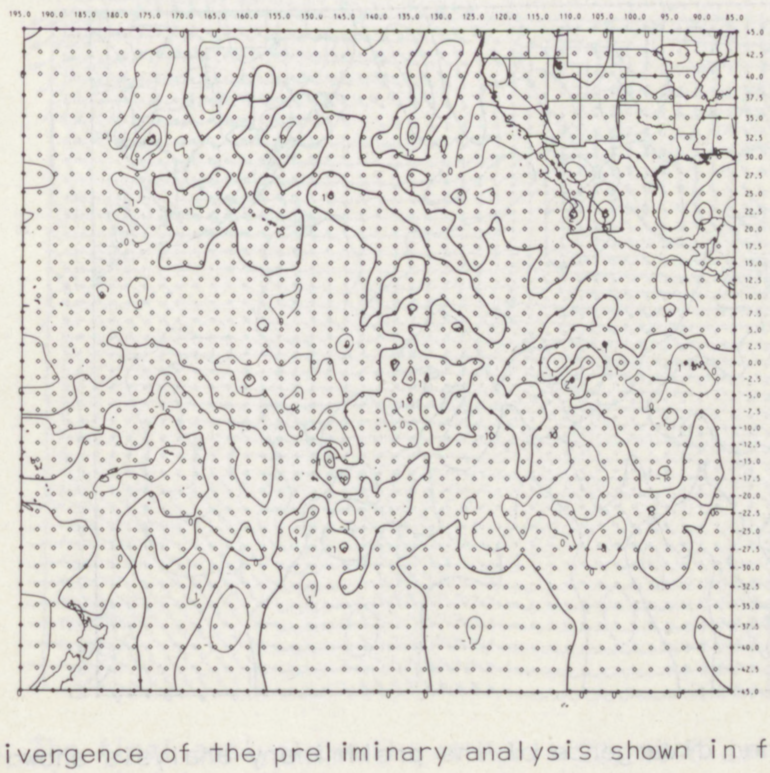

Figure 17. Divergence of the preliminary analysis shown in figure 15. Units are 10^{-5} sec^{-1}.

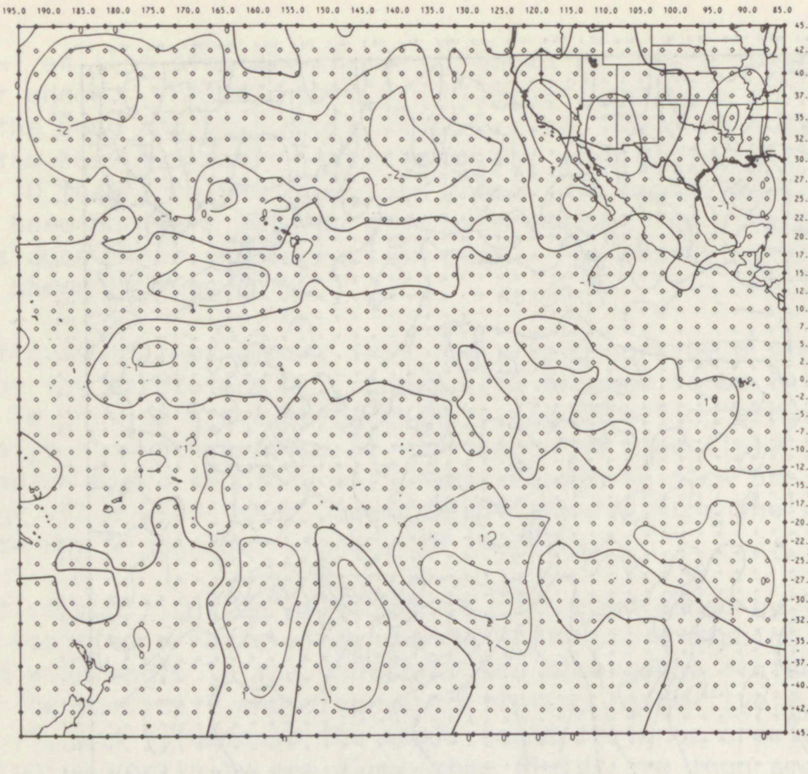

Figure 18. Smoothed vorticity of the preliminary analysis shown in figure 15. Units are 10^{-5} sec^{-1}.

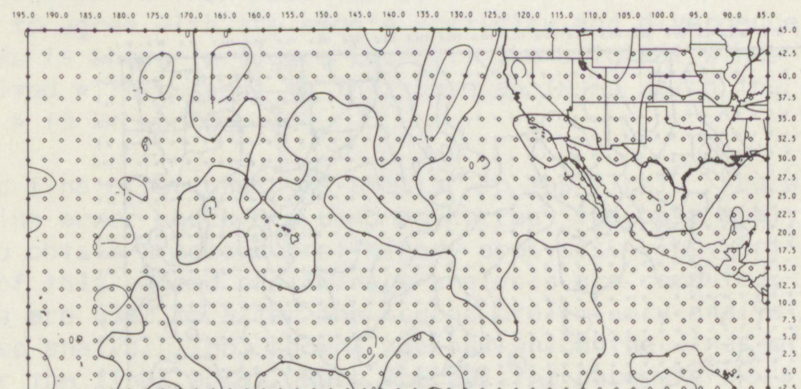

Figure 19. Smoothed divergence of the preliminary analysis shown in figure 15. Units are 10^{-5} sec^{-1}.

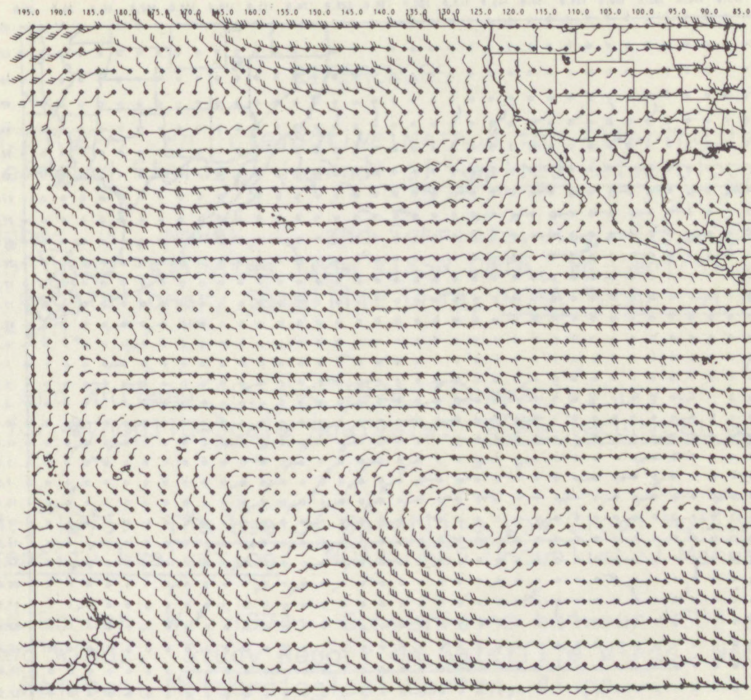

Figure 20. Base analysis for the first fine error check, constructed by modifying the preliminary analysis shown in figure 15 to conform to the smooth vorticity and divergence fields shown in figures 18 and 19 respectively.

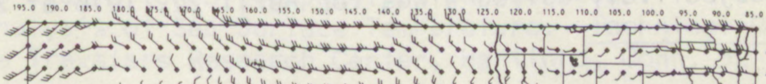

Figure 21. The final analysis valid at April 22, 1976 at 2000 GMT, constructed from the base analysis of the second fine error check (similar to figure 20) and the winds from figure 10 that survived the editing procedure.

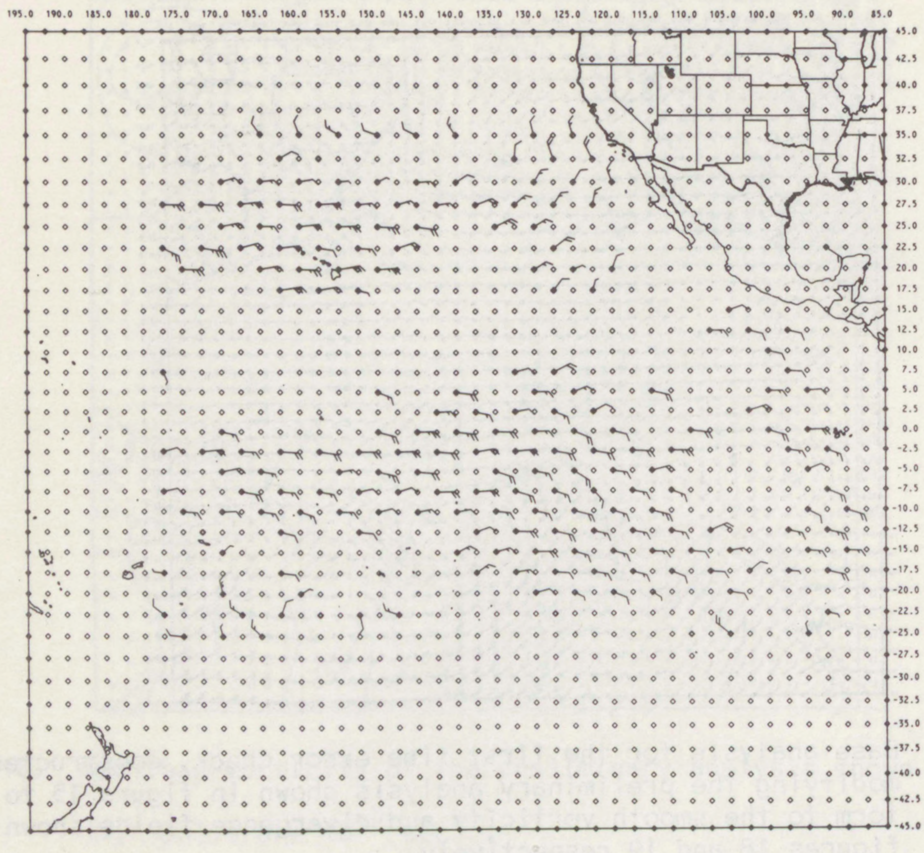

Figure 22. The objectively edited winds for April 22, 1976 at 2000 GMT.

REFERENCES

Endlich, R. M., 1967: An Interactive Method for Altering the Kinematic Properties of Wind Fields. Journal of Applied Meteorology, 6, 837-844.

Green, R., Hughes, G., Novak, C. and Schrietz, R., 1975: The Automatic Extraction of Wind Estimates from VISSR Data, in Central Processing and Analysis of Geostationary Satellite Data, NOAA Technical Memorandum NESS 64, 94-110.

Hubert, L. F., and Whitney, L. F., 1974: Compatibility of Low-Cloud Vectors and Rawins for Synoptic Scale Analysis. NOAA Technical Report NESS 70, 26 pp.

Johnson, H. M., 1976: The Use of Satellite Low Cloud Motions in Tropical Cyclone Intensity Evaluation. NOAA NESS Unpublished Manuscript.

Lemar, P., and Bonner, W., 1974: Comparisons between NESS and Wisconsin Cloud-Tracked Winds. Study Report on Satellite Winds, NASA Contract S-70252-AG, National Meteorological Center, 41 pp.

Shuman, F. G., 1957: Numerical Methods in Weather Prediction: II Smoothing and Filtering. Monthly Weather Review, 85, 357-361.

Thomasell, A., and Welsh, J. G., 1963: Studies of Techniques for the Analysis and Prediction of Temperature in the Ocean. Part I, the Objective Analysis of Sea Surface Temperature. Technical Report 7046-70, The Travelers Research Center, Hartford, Conn. 52 pp.

Thomasell, A., Harris, R. G. and Welsh, J. G., 1966: Studies of Techniques for the Analysis and Prediction of Temperature in the Ocean, Part III, Automated Analysis and Prediction. Tech Report 7421-213, The Travelers Research Center, Hartford, Connecticut, 97 pp.

Thomasell, A., 1976a: Evaluation of a Balanced 300-mb Height Analysis as a Reference Level for Satellite-Derived Soundings, NOAA Technical Report NESS 73, 25 pp.

Thomasell, A., 1976b: Objective Editing of Automated, Low-level Cloud Motion Wind Vectors from Geostationary Satellites. Proceedings of Nineteenth Plenary Meeting COSPAR.

Whitney, L. F., 1975: Personal Communication. National Environmental Satellite Service.

APPENDIX A

The Spherical Coordinate System

Analysis computations are performed with respect to the spherical coordinate grid system shown in Figure A-1. The grid points are identified by the indices I, J, where I increases downward and J increases to the right. The latitude and longitude of the upper left corner gridpoint are Θ_s and λ_s, respectively. Latitude Θ increases upward and longitude λ increases to the left. Grid spacing is defined by $\Delta\Theta$ in degrees latitude and by $\Delta\lambda$ in degrees longitude; corresponding values of grid spacing in terms of distance on the earth's surface are Δy and Δx.

Latitude and longitude are related to the grid indices by the equations

$$\Theta(I) = \Theta_s - (I-1)\,\Delta\Theta$$

and

$$\lambda(J) = \lambda_s - (J-1)\,\Delta\lambda$$

Further,

$$\Delta X(\Theta) = \frac{R\Pi}{180}\,\Delta\lambda\,\mathrm{Cos}\,\Theta$$

and

$$\Delta Y = \frac{R\Pi}{180}\,\Delta\Theta$$

where R is the radius of the Earth.

In this system divergence is calculated by

$$\begin{aligned} DIV(I,J) = &\,[u(I,J+1)-u(I,J-1)]/2\Delta x(\Theta) \\ &+ [v(I-1,J)-v(I+1,J)]/2\Delta y \\ &- v(I,J)\,\mathrm{TAN}\,\Theta/R, \end{aligned}$$

and vorticity by

$$\begin{aligned} VORT(I,J) = &\,[v(I,J+1)-v(I,J-1)]/2\Delta x(\Theta) \\ &- [u(I-1,J)-u(I+1,J)]/2\Delta y \\ &+ u(I,J)\,\mathrm{Tan}\,\Theta/R, \end{aligned}$$

where u and v are the wind components with u positive eastward and v positive northward.

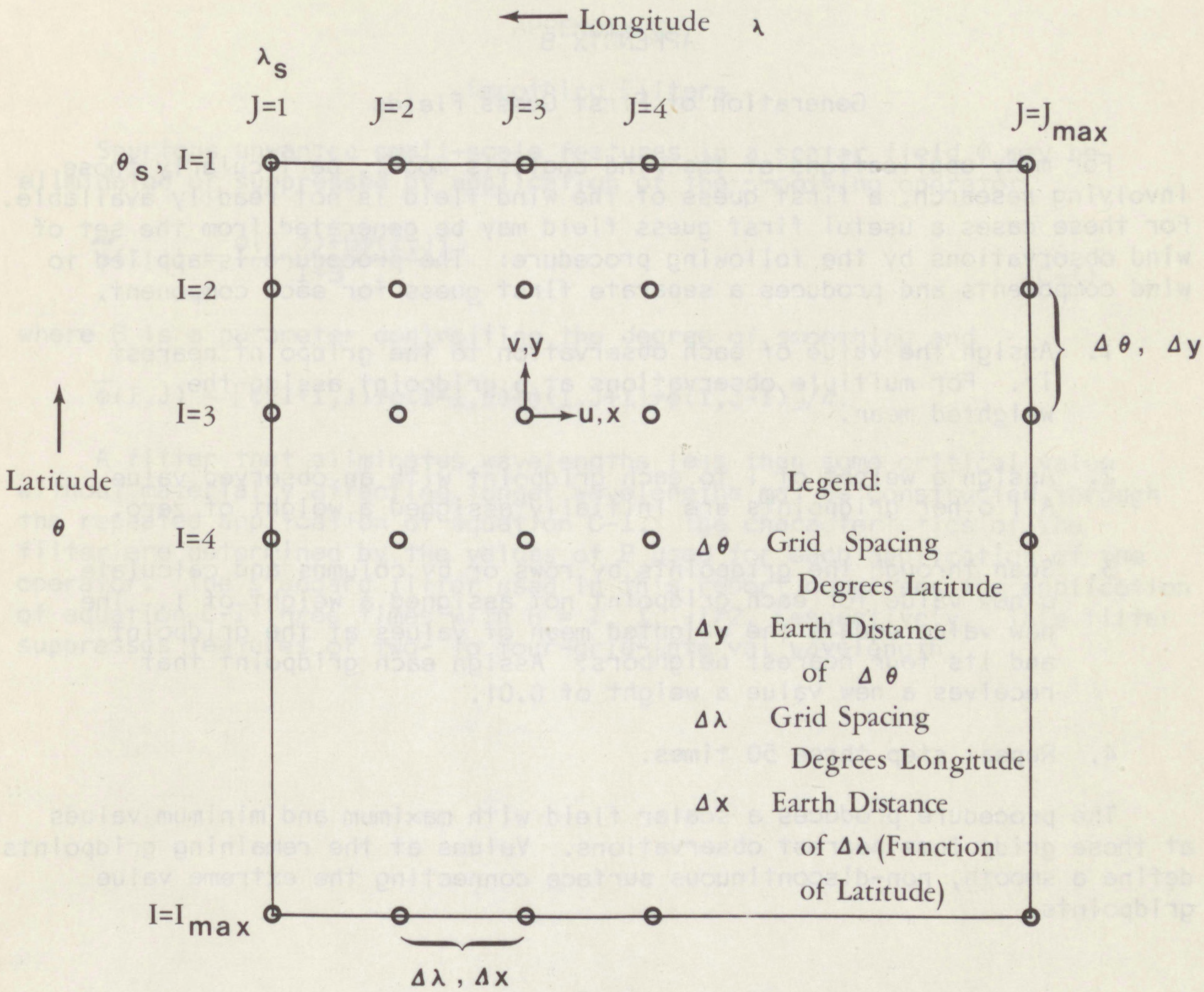

Figure A-1. The spherical coordinate grid system.

APPENDIX B

Generation of First Guess Fields

For many applications of the wind analysis model, particularly those involving research, a first guess of the wind field is not readily available. For these cases a useful first guess field may be generated from the set of wind observations by the following procedure: The procedure is applied to wind components and produces a separate first guess for each component.

1. Assign the value of each observation to the gridpoint nearest it. For multiple observations at a gridpoint assign the weighted mean.

2. Assign a weight of 1 to each gridpoint with an observed value. All other gridpoints are initially assigned a weight of zero.

3. Scan through the gridpoints by rows or by columns and calculate a new value for each gridpoint not assigned a weight of 1. The new value equals the weighted mean of values at the gridpoint and its four nearest neighbors. Assign each gridpoint that receives a new value a weight of 0.01.

4. Repeat step three 50 times.

The procedure produces a scalar field with maximum and minimum values at those gridpoints nearest observations. Values at the remaining gridpoints define a smooth, non-discontinuous surface connecting the extreme value gridpoints.

APPENDIX C

Smoothing Filters

Spurious unwanted small-scale features in a scalar field ϕ may be eliminated or suppressed by application of the smoothing operator

$$\tilde{\phi}(I,J) = \frac{\phi(I,J)+B\bar{\phi}(I,J)}{1+B} \qquad (C\text{-}1)$$

where B is a parameter controlling the degree of smoothing and

$$\bar{\phi}(I,J) = [\phi(I+1,J)+\phi(I-1,J)+\phi(I,J+1)+\phi(I,J-1)]/4.$$

A filter that eliminates wavelengths less than some critical value without materially affecting longer wavelengths may be constructed through the repeated application of equation C-1. The characteristics of the filter are determined by the values of B used for each application of the operator. The standard filter used in this report comprises the application of equation C-1 three times with B = 1, 1, -1/2, respectively. This filter suppresses features of two- to four-grid-interval wavelength.

(Continued from inside front cover)

NOAA Technical Reports

NESS 55 The Use of Satellite-Observed Cloud Patterns in Northern Hemisphere 500-mb Numerical Analysis. Roland E. Nagle and Christopher M. Hayden, April 1971, 25 pp. plus appendixes A, B, and C. (COM-73-50262)

NESS 57 Table of Scattering Function of Infrared Radiation for Water Clouds. Giichi Yamamoto, Masayuki Tanaka, and Shoji Asano, April 1971, 8 pp. plus tables. (COM-71-50312)

NESS 58 The Airborne ITPR Brassboard Experiment. W. L. Smith, D. T. Hilleary, E. C. Baldwin, W. Jacob, H. Jacobowitz, G. Nelson, S. Soules, and D. Q. Wark, March 1972, 74 pp. (COM-72-10557)

NESS 59 Temperature Sounding From Satellites. S. Fritz, D. Q. Wark, H. E. Fleming, W. L. Smith, H. Jacobowitz, D. T. Hilleary, and J. C. Alishouse, July 1972, 49 pp. (COM-72-50963)

NESS 60 Satellite Measurements of Aerosol Backscattered Radiation From the Nimbus F Earth Radiation Budget Experiment. H. Jacobowitz, W. L. Smith, and A. J. Drummond, August 1972, 9 pp. (COM-72-51031)

NESS 61 The Measurement of Atmospheric Transmittance From Sun and Sky With an Infrared Vertical Sounder. W. L. Smith and H. B. Howell, September 1972, 16 pp. (COM-73-50020)

NESS 62 Proposed Calibration Target for the Visible Channel of a Satellite Radiometer. K. L. Coulson and H. Jacobowitz, October 1972, 27 pp. (COM-73-10143)

NESS 63 Verification of Operational SIRS B Temperature Retrievals. Harold J. Brodrick and Christopher M. Hayden, December 1972, 26 pp. (COM-73-50279)

NESS 64 Radiometric Techniques for Observing the Atmosphere From Aircraft. William L. Smith and Warren J. Jacob, January 1973, 12 pp. (COM-73-50376)

NESS 65 Satellite Infrared Soundings From NOAA Spacecraft. L. M. McMillin, D. Q. Wark, J.M. Siomkajlo, P. G. Abel, A. Werbowetzki, L. A. Lauritson, J. A. Pritchard, D. S. Crosby, H. M. Woolf, R. C. Luebbe, M. P. Weinreb, H. E. Fleming, F. E. Bittner, and C. M. Hayden, September 1973, 112 pp. (COM-73-50936/6AS)

NESS 66 Effects of Aerosols on the Determination of the Temperature of the Earth's Surface From Radiance Measurements at 11.2 m. H. Jacobowitz and K. L. Coulson, September 1973, 18 pp. (COM-74-50013)

NESS 67 Vertical Resolution of Temperature Profiles for High Resolution Infrared Radiation Sounder (HIRS). Y. M. Chen, H. M. Woolf, and W. L. Smith, January 1974, 14 pp. (COM-74-50230)

NESS 68 Dependence of Antenna Temperature on the Polarization of Emitted Radiation for a Scanning Microwave Radiometer. Norman C. Grody, January 1974, 11 pp. (COM-74-50431/AS)

NESS 69 An Evaluation of May 1971 Satellite-Derived Sea Surface Temperatures for the Southern Hemisphere. P. Krishna Rao, April 1974, 13 pp. (COM-74-50643/AS)

NESS 70 Compatibility of Low-Cloud Vectors and Rawins for Synoptic Scale Analysis. L. F. Hubert and L. F. Whitney, Jr., October 1974, 26 pp. (COM-75-50065/AS)

NESS 71 An Intercomparison of Meteorological Parameters Derived From Radiosonde and Satellite Vertical Temperature Cross Sections. W. L. Smith and H. M. Woolf, November 1974, 13 pp. (COM-75-10432)

NESS 72 An Intercomparison of Radiosonde and Satellite-Derived Cross Sections During the AMTEX. W. C. Shen, W. L. Smith, and H. M. Woolf, February 1975, 18 pp. (COM-75-10439/AS)

NESS 73 Evaluation of a Balanced 300-mb Height Analysis as a Reference Level for Satellite-Derived soundings. Albert Thomasell, Jr., December 1975, 25 pp. (PB-253-058)

NESS 74 On the Estimation of Areal Windspeed Distribution in Tropical Cyclones With the Use of Satellite Data. Andrew Timchalk, August 1976, 41 pp. (PB-261-971)

NESS 75 Guide for Designing RF Ground Receiving Stations for TIROS-N. John R. Schneider, December 1976, 126 pp. (PB-262-931)

NESS 76 Determination of the Earth-Atmosphere Radiation Budget from NOAA Satellite Data. Arnold Gruber, November 1977, 31 pp. (PB-279-633)

NOAA SCIENTIFIC AND TECHNICAL PUBLICATIONS

The National Oceanic and Atmospheric Administration was established as part of the Departmen Commerce on October 3, 1970. The mission responsibilities of NOAA are to assess the socioeconomic im of natural and technological changes in the environment and to monitor and predict the state of the solid Ea the oceans and their living resources, the atmosphere, and the space environment of the Earth.

The major components of NOAA regularly produce various types of scientific and technical infor tion in the following kinds of publications:

PROFESSIONAL PAPERS — Important definitive research results, major techniques, and special investigations.

CONTRACT AND GRANT REPORTS — Reports prepared by contractors or grantees under NOAA sponsorship.

ATLAS — Presentation of analyzed data generally in the form of maps showing distribution of rainfall, chemical and physical conditions of oceans and atmosphere, distribution of fishes and marine mammals, ionospheric conditions, etc.

TECHNICAL SERVICE PUBLICATIONS — Reports containing data, observations, instructions, etc. A partial listing includes data serials; prediction and outlook periodicals; technical manuals, training papers, planning reports, and information serials; and miscellaneous technical publications.

TECHNICAL REPORTS — Journal quality with extensive details, mathematical developments, or data listings.

TECHNICAL MEMORANDUMS — Reports of preliminary, partial, or negative research or technology results, interim instructions, and the like.

Information on availability of NOAA publications can be obtained from:

ENVIRONMENTAL SCIENCE INFORMATION CENTER (D822)
ENVIRONMENTAL DATA AND INFORMATION SERVICE
NATIONAL OCEANIC AND ATMOSPHERIC ADMINISTRATION
U.S. DEPARTMENT OF COMMERCE

6009 Executive Boulevard
Rockville, MD 20852

NOAA--S/T 78-267